MEASUREMENT SCIENCE REVIEW

Experimental Study on EHD Flow Transition in a Small Scale Wire-plate ESP

Chuan Wang [1], ZhenqiangXie[1], Binggui Xu [2], Jun Li[1], Xu Zhou[1]

[1]*School of Mechanical and Electrical Engineering, Southwest Petroleum University, Xindu Avenue, No.8, 610500, Chengdu, China, cwang_swpu@163.com*
[2]*Drilling Mechanical Department, CNPC Drilling Research Institute, Huanghe Street, No.5, 102206, Beijing, China*

The electrohydrodynamic (EHD) flow induced by the corona discharge was experimentally investigated in an electrostatic precipitator (ESP). The ESP was a narrow horizontal Plexiglas box (1300 mm×60 mm×60 mm). The electrode set consisted of a single wire discharge electrode and two collecting aluminum plate electrodes. Particle Image Velocimetry (PIV) method was used to visualize the EHD flow characteristics inside the ESP seeded with fine oil droplets. The influence of applied voltage (from 8 kV to 10 kV) and primary gas flow (0.15 m/s, 0.2 m/s, 0.4 m/s) on the EHD flow transition was elucidated through experimental analysis. The formation and transition of typical EHD flows from onset to the fully developed were described and explained. Experimental results showed that the EHD flow patterns change depends on the gas velocity and applied voltage. EHD flow starts with flow streamlines near collecting plates bending towards the wire electrode, forming two void regions. An oscillating jet forming the downstream appeared and moved towards the wire electrode as voltage increased. For higher velocities (≥0.2 m/s), the EHD transition became near wire phenomenon with a jet-like flow structure near the wire, forming a void region behind the wire and expanding as voltage increased. Fully developed EHD secondary flow in the form of counter-rotating vortices appeared upstream with high applied voltage.

Keywords: Electrostatic precipitator, electrohydrodynamics, particle image velocimetry, flow transition, air-fine oil droplets separation.

1. INTRODUCTION

Electrostatic precipitators (ESPs) are air cleaning devices used to remove particles from gas flows with electrical forces and have been widely used for several decades. Wire-plate ESPs are one of the most commonly used types, which consist of several discharge wires connected to the high power supply and grounded plates to collect the hazardous particles. The principles of ESP operation are well explained by many literatures [1], [2]. The applied voltages are kept high enough to ionize the gas around the wires. The charges (electrons or ions) generated by corona discharge are driven towards the grounded plates due to the electrical forces. The collisions of charges with gas molecules create a momentum transfer to the gas molecules, providing a driving force to the fluid and causing an electrohydrodynamic (EHD) secondary flow. Its characteristics are the least understood phenomena inside ESPs because of the mutual interaction of the primary gas flow field, the electric field disturbed by corona discharge, the particle charging and transport.

In order to investigate the EHD flow field, particles motion and precipitation, both experimental and numerical efforts have been carried out. Liang and Lin [3] have numerically simulated the characteristics of ionic wind and its effect on

the ESP performance. They indicated that the ionic wind becomes pronounced and has a significant influence on the flow field and the collection efficiency when gas flow velocity is less than 0.6 m/s. Seok and Sang [4] conducted an experimental study on the EHD flow and particle transport mechanism with Alumina (Al_2O_3) particles using Laser Doppler Anemometry (LDA) inside an ESP model composed of plates with a cavity. They found that gas velocities of the core flow and the circulating flow inside the cavity increased due to the corona wind for increasing corona voltage. When the flow with high inlet turbulence intensity entered the ESP, the collection efficiency was higher compared with the case of relatively lower inlet turbulence intensity below a critical corona voltage. Mizeraczyk et al. [5] studied the velocity field of flue gas flow seeded with cigarette smoke inside ESP using the Particle Image Velocimetry (PIV) method. They measured the secondary EHD flow velocity near the discharge region and demonstrated that the secondary flow has significant impact on the motion and collection of small particles, mainly in the submicron range. Comprehensive investigations of EHD velocity field in wire-plate ESP have been published by Podlinski et al. [6]-[9] using 2D and 3D PIV techniques. The typical flow patterns for cylinder and wire plate geometries under various applied voltages were experimentally characterized using PIV [10]. Chang et al.

[11] established an EHD flow regime map for the wire-plate geometry ESPs under a large range of primary gas flow and applied voltages and defined four typical EHD flow patterns for negative and positive polarity, respectively. Franoosh et al. [12] analyzed the EHD turbulent flow and mono-disperse charged particle transport and collection in a wire-plate ESP by the 3D numerical method. Kawakami et al. [13] studied the performance characteristics between horizontally and vertically oriented electrodes EHD ESP for collection of low-resistive diesel particulates. Li et al. [14] simulated the high-temperature effect on EHD characteristics in a wire-plate electrostatic precipitator by the CFD method.

Despite the numerous publications and study contributions mentioned above, the EHD flow has not been fully understood yet. Most of the studies focused on the EHD flow distribution and its impacts on the collection efficiency and particle transport. However, the EHD flow transition and the physics behind it have not been well explained. And for most of the recent visualization studies, the primary gas flow was seeded with solid particles, such as dust, fly ash and cigarette smoke, etc. The flow visualization of EHD flow field for liquid droplets separation is very limited and has not been implemented thoroughly as in dust separation because of the complexity of droplets behavior under electrostatic field. The purpose of this paper is to investigate the complicated EHD flow characteristics and flow transition under different operating conditions. PIV method, which has been confirmed that it can provide good insight of coupled electric field and flow field, is introduced for the visualization study. EHD flow patterns and transition are presented and explained when the primary gas flow is seeded with fine oil droplets. The flow patterns obtained in this study are also compared with previous studies for which the gas flows were seeded with solid particles.

2. EXPERIMENTAL SETUP

The wire-plate ESP used for this study was mounted in a narrow horizontal Plexiglas box (1300 mm×60 mm×60 mm) (Fig.1.). Two collecting aluminum plates (220 mm long, 60 mm wide and 2 mm thick) were placed parallel at the top and bottom of the Plexiglas channel with the distance of 60 mm. The discharge wire electrode (diameter of 0.2 mm and 60 mm long) was set in the middle of the precipitator. In order to obtain fully developed primary flow, the distance between the entrance of the duct and the wire electrode was 1110 mm. The electrode wire was connected to a high voltage power supply providing a DC positive voltage through a 10 MΩ resistor. The collecting aluminum plates were grounded. The square horizontal duct was connected to an atomizer which generates oil droplets with the average diameter of 2 μm. Air flow seeded with oil droplets was blown along the ESP at room temperature (T=20°C) and atmospheric pressure.

The pulsed Nd:YAG laser (*P*=200 mW, *λ*=532 nm) was employed for illuminating the housing in the form of a laser sheet. The laser sheet in vertical position was adjusted along the flow direction in the plane perpendicular to the wire electrode at its half-length. The image of the 2D concentration distribution was then recorded by the CCD camera placed perpendicularly to the laser sheet. The area of the measured velocity field was 220 mm×60 mm. Full-frame images were acquired and transferred to a processing computer. Both instantaneous and time averaged flow images under different condition were provided. The 2D PIV image was interrogated using cross-correlation analysis in 32×32 pixel sub-images with an overlap of 50 % between adjacent interrogations. The average particle velocities presented here were calculated using 100 coupled images. In Raffle et al. [15], a detailed discussion on cross-correlation analysis and time averaging method are given. The spurious vectors calculated and based on the local median filtering were less than 3 %. No smoothing data were used for the velocity calculation.
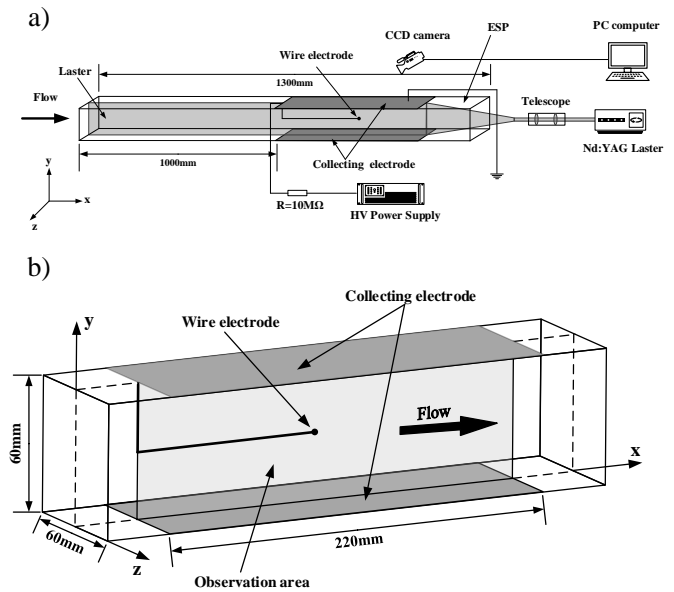

Fig.1. a) Schematic of experimental set-up; b) ESP with observation area marked.

3. DIMENSIONLESS ANALYSIS: THE INTERACTIONS OF GAS FLOW FIELD AND ELECTRIC FIELD

The transport of particles inside ESPs mainly depends on the balance between the electric force and the inertial forces. The interactions between electrohydrodynamic number (Ehd) and Reynolds number (Re) squared (Ehd/Re²) is used to analyze the interactions of electric field and primary gas flow field [16], which describes the ratio of the electric forces to the inertial force. The Reynolds number can be obtained by:

$$\mathrm{Re} = \frac{U_0 l}{v} \quad (1)$$

where U_0 is the mean gas velocity, l=0.06 m is the characteristic length (plate–plate distance), and v is the air kinematic viscosity (v=1.57×10⁻⁵ m²/s).

The Ehd can be calculated by the following formula:

$$\mathrm{Ehd} = \frac{I \times l^3}{v^2 \times \rho \times \mu_i \times A} \quad (2)$$

where I is the average total discharge current; ρ is the air density (1.2 kg/m^3); μ_i is the ion mobility (6.45×10^{-5}m^2/Vs); A is the discharge area equal to the doubled area of the collecting aluminum plates (for this geometry A=7.2×10^{-3} m^2). Based on the dimensionless analysis of the Navier-Stokes Equation [10], the EHD secondary flow becomes significant when Ehd/Re^2≥1.

4. RESULTS AND DISCUSSION

A. Current and voltage characteristics

The measured corona current–voltage characteristics (CVC) of the ESP model under different operating conditions are shown in Fig.2. The CVC under static condition, which means there was no primary gas flow and no oil droplets inside the ESP, showed a parabolic relationship between current and applied voltage. The corona onset voltage was about 8 kV. When the gas flows were seeded with oil droplets, the electric field behaved differently compared with the result under static condition, see the CVC of 0.15 m/s, 0.2 m/s and 0.4 m/s. As expected, the impact of gas velocities on the electric field was negligible due to the mobility of gaseous ions which is hundred times higher than the mobility of the charged particles. In practice, the measured total current, equal to the integral of current density on the collecting plates, is determined by the drift of gaseous ions only, since the mobility of charged particles is much lower [14]. When oil droplets are present, the amount of drift ions to the plates is lower compared with the absence of droplets because of charging particles. Therefore, when seeded with oil droplets, the current was lower than static condition at the same applied voltages.
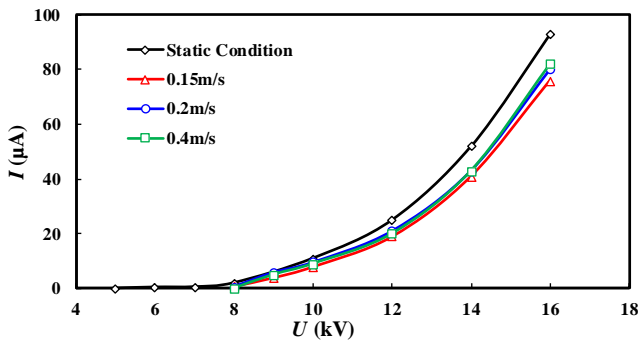

Fig.2. Current–voltage characteristics under different operating conditions.

B. EHD flow transition

The visualization results presented included both instantaneous images taken by the CCD camera and time averaged images by taking the average of 120 instantaneous images. Fig.3. indicated the flow characteristics when no voltage was applied and the mean gas velocity U_0 was 0.15 m/s. The bright dot placed in the middle is the wire electrode and the two boundaries in the top and bottom are the collecting plates. The flow is blown from left to right and the dark line in the left center of the duct is the shadow of the wire electrode. The existence of oil smoke in the illuminating

plane is revealed by the gray regions, while the absence of oil droplets is detected as dark regions. Therefore, relative oil droplets concentration can be quantified by the gray level recorded in these images. Fig.4. shows the averaged flow velocity field and corresponding flow streamline when no voltage was applied (Ehd/Re^2=0). Typical laminar flow is observed in the duct and the wakes behind the wire are too small to be observed in the PIV images.
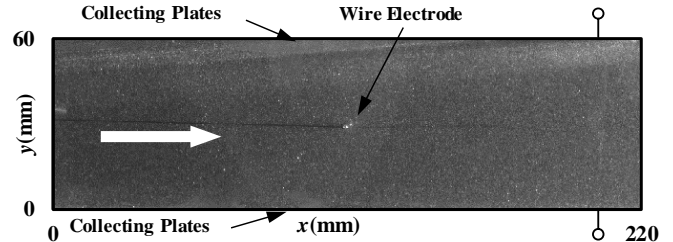

Fig.3. Instantaneous flow field image with no applied voltage (U_0=0.15 m/s).
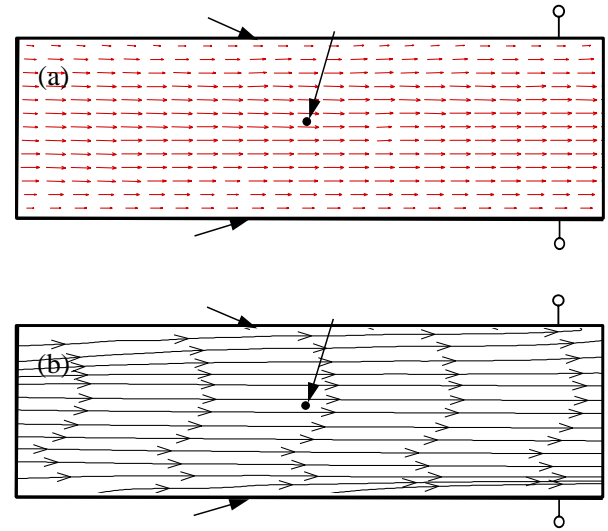

Fig.4. a) Averaged flow velocity field; b) Corresponding flow streamline when no voltage was applied (U_0=0.15 m/s).

Fig.5. illustrates the EHD flow transition near corona onset voltage (8~9 kV) at relatively low gas velocity (U_0=0.15 m/s, Re=573). The left column images are the instantaneous results of EHD flow patterns, and the right column ones are the corresponding time averaged results. It is worthy to mention that the results presented in this study differ slightly from the gas flow field. The drift velocity of the charged droplets should be subtracted from the total velocity in order to get the EHD flow patterns inside the ESP. However, the drift velocity induced by the electric force is considerably smaller than the gas velocity in the whole ESP duct except in the area near the corona wire. Thus, the EHD flow patterns can be reasonably well represented by the droplets flow patterns presented here [17]. For V=8 kV, as shown in Fig.5.a), the flow did not show much change compared with Fig.3. (no voltage applied). In this case the airflow dominates the flow field, Ehd/Re^2=2.2. When the applied voltage

reached 8.2 kV, $Ehd/Re^2=4.1$, the electric field started to modify the flow field. The streamlines are almost parallel to the collecting plates, while bending towards the wire electrode near the collecting plates, creating two "void" regions, see Fig.5.b). This pattern qualitatively supported the findings of past numerical investigations by Lei et al. [18] and Zhao [19]. Such a phenomenon has also been observed by Leonard [20]. However, the formation of this EHD pattern has not been explained so far and few of the recent visualization studies with solid particles provided in the introduction part mentioned the existence of this flow pattern. As it is well known, the EHD can modify the turbulence structures in ESPs. Based on Lei's numerical study [18], for a single wire-plate ESP there are two turbulence zones inside ESP when a high voltage is applied. One is near the impinging point on the walls (collecting plates), the other one is near the corona wire. When there is no externally forced flow, the turbulent energy is higher near the wire than on the wall. However, the cross-flow can weaken the velocity gradient caused by the Coulomb force. So the turbulent kinetic energy decreases with the increase of the inlet gas velocity. Thus, the high turbulence zones are not near the wire any more, but near the plates.

The "void" regions shrink inwards closer to the collecting plates when the inlet velocity increases. As expected, there is no such phenomenon in Fig.6. and Fig.7. because of the increase of the inlet velocity. The main reason for the formation of the void regions is the turbulence kinetic energy under the mutual interactions of electric field and gas flow field. As the applied voltage increased to 8.4 kV, an oscillating jet appeared from downstream, see Fig.5.c).
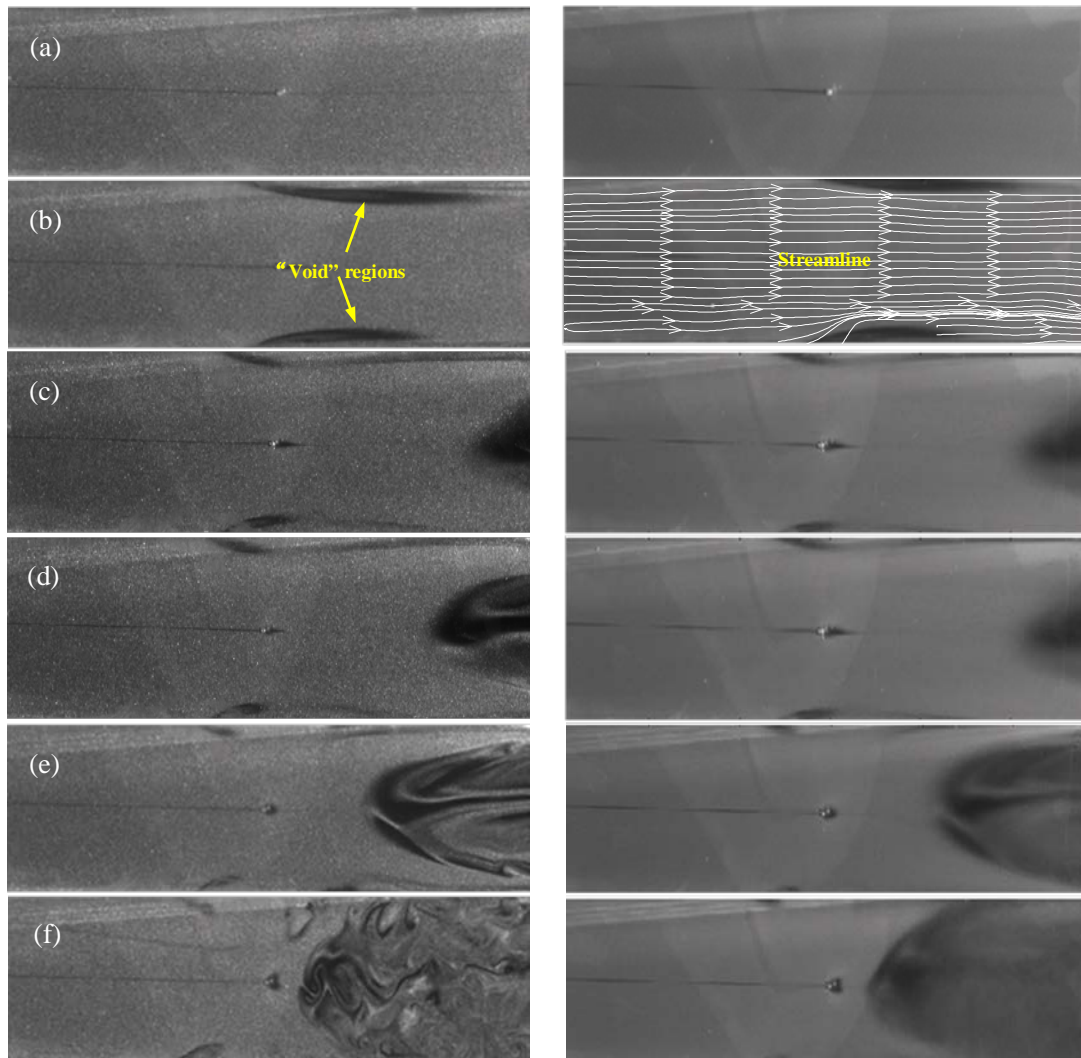

Fig.5. EHD flow transition near the corona onset (U_0=0.15 m/s). a): V=8 kV, Ehd/Re^2=2.2; b) V=8.2 kV, Ehd/Re^2=4.1; c) V=8.4 kV, Ehd/Re^2=5.8; d) V=8.8 kV, Ehd/Re^2=9.2; e) V=9 kV, Ehd/Re^2=11; f) V=9.8 kV, Ehd/Re^2=19.

Meanwhile, the two void regions are filled with droplets and become unobvious because of the higher electric field near the corona wire, pushing the droplets towards the collecting plates under the influence of the Coulomb force. During the experiment, the droplets near the wire moved to the plates in the form of a jet. However, the jet near the wire is not clear in

this study. This can be attributed to the higher concentration of the oil droplets, inducing a higher drag force. The formation of the jet in the downstream can be explained by the pressure drop during the corona discharge, which has been confirmed by Yabe's experimental study [21]. As the voltage increases, Fig.5.d) and Fig.5.e), the jet moves towards the wire and becomes bigger and bigger, and the flow in the downstream becomes more and more turbulent.

For higher primary gas flow velocity, the effect of EHD becomes near-wire phenomenon, see Fig.6. and Fig.7. Fig.6. illustrates the EHD flow transition near corona onset voltage for U_0=0.2 m/s. No significant changes of the EHD flow were observed when the applied voltage was lower than 9 kV (results not shown here). One jet forms near the wire towards the downstream at 9 kV, corresponding Ehd/Re^2=9.3, as shown in Fig.6.a). This kind of EHD flow pattern has been observed by many authors [4], [17], [22].
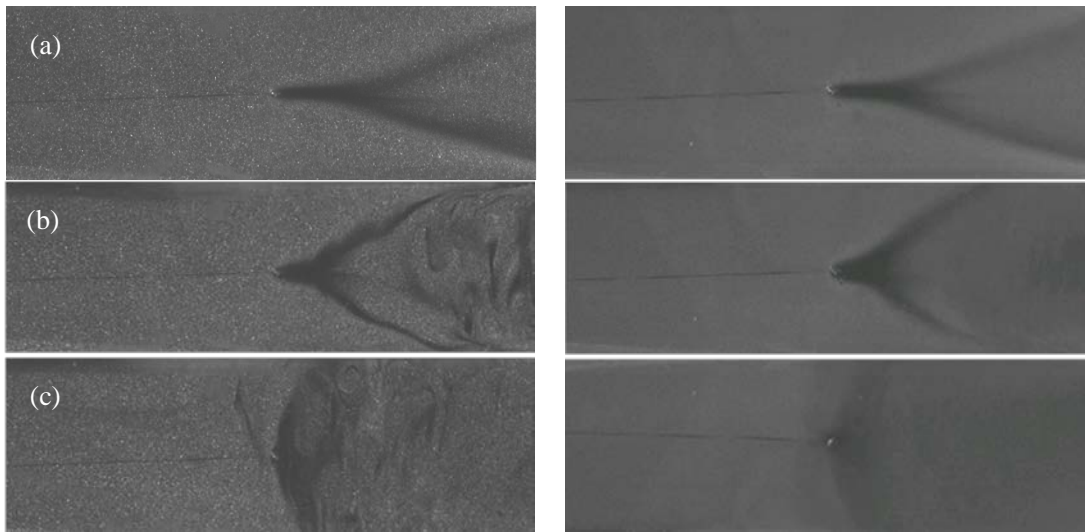

Fig.6. EHD flow transition near the corona onset (U_0=0.2 m/s). a) V=9 kV, Ehd/Re^2=9.3; b) V=9.5 kV, Ehd/Re^2= 12.5; c) V=9.8 kV, Ehd/Re^2= 14.4.
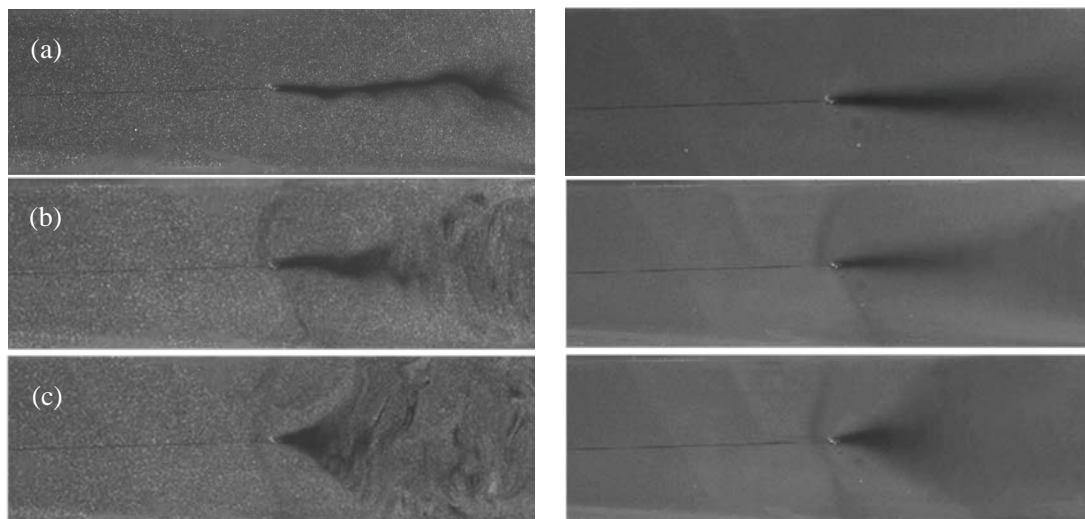

Fig.7. EHD flow transition near the corona onset (U_0=0.4 m/s). a) V=9 kV, Ehd/Re^2=2; b) V=9.5 kV, Ehd/Re^2= 2.8; c) V=9.8 kV, Ehd/Re^2=3.2.
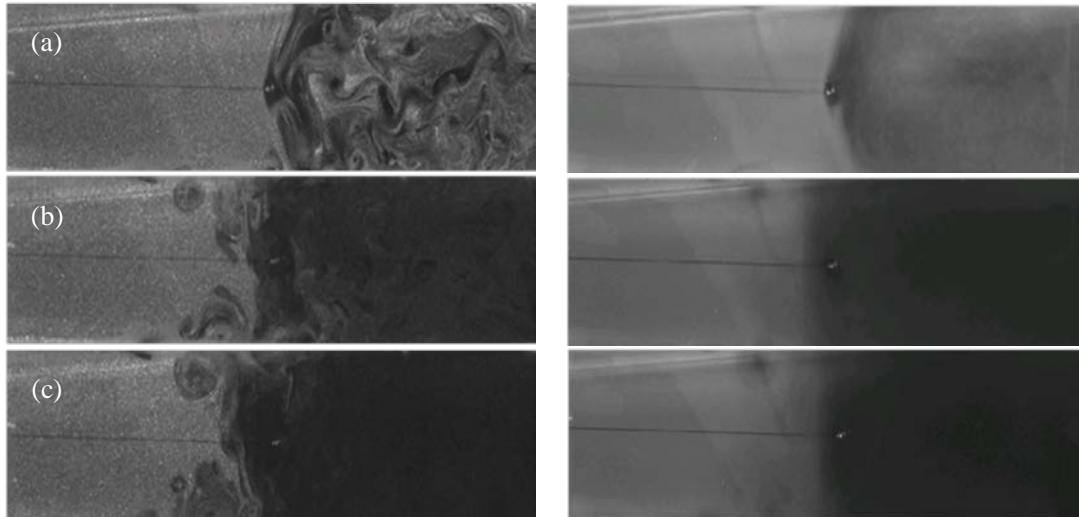
Fig.8. EHD flow transition at high applied voltage (U_0=0.15 m/s). a) V=10 kV, Ehd/Re^2=21.3;
b) V=14 kV, Ehd/Re^2= 112.3; c) V=16 kV, Ehd/Re^2= 209.8.
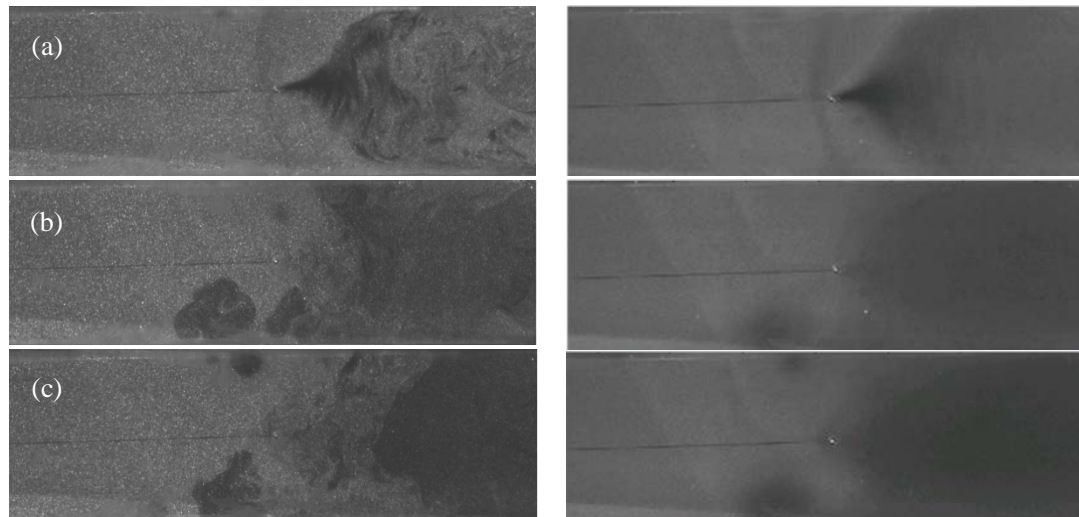

Fig.9. EHD flow transition at high applied voltage (U_0=0.4 m/s). a) V=10 kV, Ehd/Re^2=3.5;
b) V=14 kV, Ehd/Re^2= 16.9; c) V=16 kV, Ehd/Re^2= 32.2.

Because of the higher electric field in the vicinity of the discharge wire, the charged droplets in this area are pushed towards the collecting plates, thus forming such jet-like EHD flow pattern and a droplet free zone behind the discharge wire. The "mouth" of the jet and the turbulent intensity of the downstream increases with the increase of applied voltage, because the migration velocity of the charged droplets increases as applied voltages increase. Fig.7. shows the same trend as observed in Fig.6. At the same applied voltage, it is obvious that the EHD effect is stronger for primary flow velocity U_0=0.2 m/s (Fig.6.) than for U_0=0.4 m/s (Fig.7.). It can be concluded that the cross flow acted to suppress the formation of EHD flow as higher cross airflows with larger convective forces depress the corona wind. It can be predicted that the electric influence would be masked if the inlet airflow exceeds a critical value. It is worthy to mention that the main

air flow sweeps the charges to the downstream side of the wire, causing higher electric-field region in the downstream.

Fig.8. and Fig.9. show the transition of EHD flow pattern under high applied voltage (from 10 kV to 16 kV) at primary flow velocity 0.15 m/s and 0.4 m/s, respectively. When the applied voltage is high, the electric force dominates the flow field. This process of transition has been discussed in our previous study and by other authors. At the same applied voltage, the EHD effects and the separation performance are stronger at 0.15 m/s than at 0.4 m/s. And when the applied voltage reached 14 kV, two counter rotating vortices formed upstream near the wire. At 16 kV fully developed EHD secondary flow in the form of large vortices blocked the main gas flow. The formation of these vortices is due to the flow continuity which demands gas return to the corona region, thus establishing a recirculating flow.
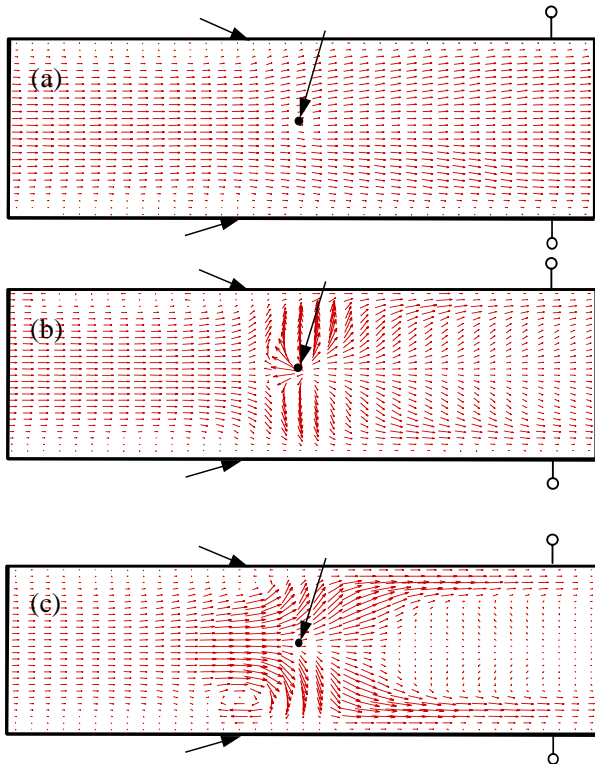
Fig.10. Averaged flow velocity fields for different applied voltages: a) V=8 kV, b) V=10 kV, c) V=16 kV. The primary gas velocity was 0.4 m/s.
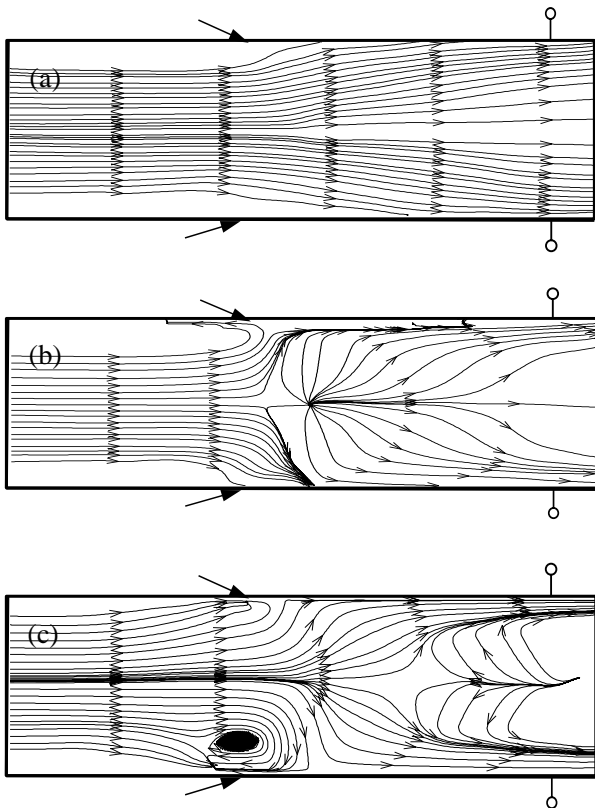

Fig.11. Averaged flow streamlines for different applied voltages: a) V=8 kV, b) V=10 kV, c) V=16 kV. The primary gas velocity was 0.4 m/s.

The results of averaged droplets flow velocity fields and corresponding flow streamlines for different applied voltages under relatively high primary gas velocity (0.4 m/s) are shown in Fig.10. and Fig.11., respectively. As can be seen clearly, after applying high voltage, the velocity field and flow streamlines changed significantly with respect to the results without applied voltage. From 8 kV to 10 kV, the effect of electric force acted mainly near the wire and downstream. The strong electric field in the vicinity of the wire pushes the droplets from the central part of ESP to the collecting plates. Droplets velocity was increased from the wire and reached the maximum value near the plates. At 16 kV, vortices formed in front of the wire, increasing the droplets velocity in the central part of the ESP, upstream of the wire electrode. Meanwhile, some reversal flows were observed in the central part of the ESP, downstream of the wire. The vortex near the bottom plate was stronger than that near the top plate. This can be explained by the gravity effect of the high loaded droplets, forming a thicker layer at the bottom during the experiment causing higher electric strength between the discharge wire and the bottom plate.

C. Comparison with EHD flows obtained with solid particles

The EHD flow seeded with fine oil droplets obtained in this study was compared with published ESP flow patterns [11] seeded with solid particles. It is not difficult to find that some differences between them exist. The EHD flow pattern in Fig.5.b) was not mentioned in the EHD flow map proposed by Chang et al. Another difference is the presence of oscillating jets which appear from the downstream, as shown in Fig.5.c) and Fig.5.d), expanding and coming closer to the wire electrode with the increase of applied voltage. However, this phenomenon was not mentioned by Chang et al. [11]. The last difference is related to the EHD von Kaman vortex, which was clearly described in a previous study [7], and did not appear in this experiment. It is interesting to mention that all the differences appear under low Ehd and low Re when both flow field and electric field are weak. The oil droplets with higher adhesive forces than that of solid particles might be the main cause of these differences.

5. CONCLUSIONS

The EHD flow field in a wire-plate ESP was experimentally studied by the PIV method. Images of the laser illuminated oil droplets taken by the CCD camera provided a good insight into the interaction between the gas flow field and the corona induced by the electric field. Experimental results showed that the EHD flow patterns changed significantly during corona discharge, depending on the gas velocity and applied voltage. EHD flow structures became significant and played a bigger role in downstream and near the wire in the presence of airflows when $Ehd/Re^2 \geqslant 1$. For lower gas velocities, the EHD flow transition near corona onset voltage is not only near wire phenomenon. EHD flow starts with flow streamlines near collecting plates bending towards the wire electrode, forming two "void" regions. An oscillating jet formed in the downstream of ESP and moved towards the wire electrode as voltage increased. Fully developed EHD

secondary flow in the form of counter-rotating vortices appeared upstream at high applied voltage, meanwhile reversal flow was observed downstream. For higher velocities of the primary flow ($\geqslant$0.2 m/s), the EHD transition is near wire phenomenon with a jet-like flow structure near the wire, forming a void region behind the wire. The jet expanded as voltage increased. The vortices and reversal flows were also observed at high applied voltage. Higher cross airflows with larger convective forces depress the corona wind and weaken the EHD flow structures at the same applied voltage. The EHD flow obtained with oil droplets showed different characteristics near corona onset voltage under low cross flow, where both electric and inertial forces are weak. The reason of the difference is probably caused by the different adhesive forces between liquid and solid particles.

REFERENCES

[1] Robinson, M. (1971). *Electrostatic Precipitation.* New York: Wiley Interscience.

[2] Oglesby, S., Nichols, G.B. (1978). *Electrostatic Precipitation.* New York: Marcel Dekker Inc.

[3] Liang, W., Lin, T. (1994). The characteristics of ionic wind and its effect on electrostatic precipitators. *Aerosol Science and Technology*, 20 (4), 330-344.

[4] Seok, J.P., Sang, S.K. (2000). Electrohydrodynamic flow and particle transport mechanism in electrostatic precipitators with cavity walls. *Aerosol Science and Technology*, 33 (3), 205–221.

[5] Mizeraczyk, J. et al. (2001). Measurements of the velocity field of the flue gas flow in an electrostatic precipitator model using PIV method. *Journal of Electrostatics*, 51–52, 272–277.

[6] Podlinski, J. et al. (2006). Electrohydrodynamic gas flow in a positive polarity wire-plate electrostatic precipitator and related dust particle collection efficiency. *Journal of Electrostatics*, 64 (3-4), 259–262.

[7] Podlinski, J. et al. (2006). 3D PIV measurements of the ehd flow patterns in a narrow electrostatic precipitator with wire-plate or wire-flocking electrodes. *Czechoslovak Journal of Physics*, 56 (Suppl. 2), B1009–B1016.

[8] Niewulis, A. et al. (2007). EHD flow measured by 3D PIV in a narrow electrostatic precipitator with longitudinal-to-flow wire electrode and smooth or flocking grounded plane electrode. *Journal of Electrostatics*, 65 (12), 728-734.

[9] Podlinski, J. et al. (2006). EHD flow in a wide electrode spacing spike–plate electrostatic precipitator under positive polarity. *Journal of Electrostatics*, 64 (7-9), 498-505.

[10] Chang, J.S. et al. (2006). On-set of EHD turbulence for cylinder in cross flow under corona discharges. *Journal of Electrostatics*, 64 (7-9), 569-573.

[11] Chang, J.S., Dekowski, J., Podlinski, J., Brocilo, D. (2005). Electrohydrodynamic gas flow regime map in a wire plate electrostatic precipitator. In *Industry Applications Conference: Fourtieth IAS Annual Meeting*, 2-6 October 2005, Hong Kong, China. IEEE, 2597-2600.

[12] Farnoosh, N., Adamiak, K., Castle, G.S.P. (2010). 3-D numerical analysis of EHD turbulent flow and mono-disperse charged particle transport and collection in a wire-plate ESP. *Journal of Electrostatics*, 68 (6), 513-522.

[13] Kawakami, H. et al. (2013). Performance characteristics between horizontally and vertically oriented electrodes EHD ESP for collection of low-resistive diesel particulates. *Journal of Electrostatics*, 71 (6), 1117-1123.

[14] Li, Y. et al. (2015). CFD simulation of high-temperature effect on EHD characteristics in a wire-plate electrostatic precipitator. *Chinese Journal of Chemical Engineering*, 23 (4), 633-640.

[15] Raffel, M., Willert, C.E., Wereley, S., Kompenhans, J. (2007). *Particle Image Velocimetry : A Practical Guide.* Springer.

[16] IEEE. (2003). Technical committee, recommended international standard for dimensionless parameters used in electrohydrodynamics. *IEEE Transactions on Dielectrics and Electrical Insulation*, 10 (1), 3–6.

[17] Podlinski, J., Niewulis, A., Mizeraczyk, J., Atten, P. (2008). ESP performance for various dust densities. *Journal of Electrostatics*, 66 (5-6), 246-253.

[18] Lei, H., Wang, L., Wu, Z. (2008). EHD turbulent flow and Monte-Carlo simulation for particle charging and tracing in a wire-plate electrostatic precipitator. *Journal of Electrostatics*, 66 (3-4), 130–141.

[19] Zhao, L., Adamiak, K. (2008). Numerical simulation of the electrohydrodynamic flow in a single wire-plate electrostatic precipitator. *IEEE Transactions on Industry Applications*, 44 (3), 683-691.

[20] Leonard G.L., Mitchner, M., Self, S.A. (1983). An experimental study of the electrohydrodynamic flow in electrostatic precipitators. *Journal of Fluid Mechanics*, 127 (1), 123–140.

[21] Yabe, A., Mori, Y., Hijikata, K. (1978). EHD study of the corona wind between wire and plate electrodes. *AIAA Journal*, 16 (4), 340-345.

[22] Kallio, G.A., Stock, D.E. (1990). Flow visualization inside a wire-plate electrostatic precipitator. *IEEE Transactions on Industry Applications*, 26 (3), 503–514.